Dual emitting $CsPbBr_3$/Eu-BDC composite as a ratiometric photoluminescent turn on probe for aliphatic amine sensing

Highlights

This chapter mainly highlights the use of a ratiometric fluorescence sensor for volatile organic amines. In an attempt to create a self-calibrating amine sensor, this chapter investigates a dual emitting fluorescent composite made from combining $CsPbBr_3$ and Eu-BDC. The results presented here establishes the suggested sensor's quick and selective turn on PL response to aliphatic organic amine derivatives. The potential of the proposed fluorescence sensor is utilized for monitoring the meat freshness. The synthesis, characterization and luminescence property study of $CsPbBr_3$/Eu-BDC composite is emphasized herein.

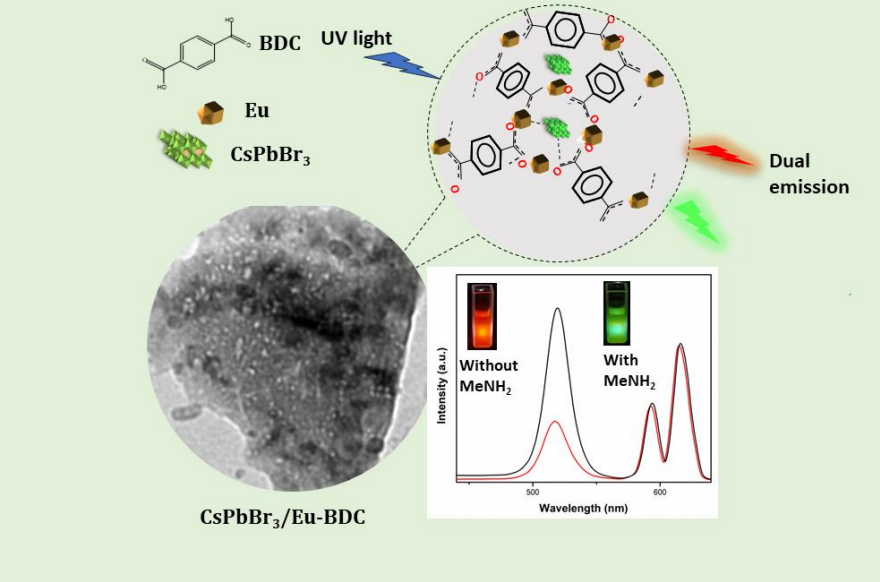

5.1. Introduction

As a result of industrialization and rising population, the issue of environmental pollution from a wide variety of organic contaminants has gained widespread attention. Volatile organic amines, a type of noxious gas, pose a major hazard to both human health and the environment. Among them, aliphatic amines are frequently used as chemical intermediates in textile industries, plastics, food and pharmaceutical sectors, which eventually find their way into the environment [1,2]. They contribute to air pollution by forming carcinogenic nitrosamines, and can induce unpleasant odors, eye and skin irritation, conjunctivitis, and corneal edema after inhalation [3]. Consequently, it is strongly advised to reduce volatile organic amine exposure into the environment. Additionally, during the disintegration of food products specially for meat and fish products, several changes such as biological, chemical, and physical changes have been occurs, which in turn convert the inside protein to their constituent amino acids. These amino acids underwent further decarboxylation to generate biogenic amines (cadaverine, putrescine and other aliphatic amines) [4]. Thus, tracking them in stored meat products is essential for determining their freshness. The need for precise determination of volatile amines and its derivatives has increased significantly in response to rising concern about the health risks by exposure to these toxic volatile organic compounds (VOCs) [3].

As was already mentioned in earlier chapters, fluorescence (FL) based sensing techniques offer a low cost, easily handled, quick time response, highly sensitive and selective analyte detection compared to conventional instrumentation approaches [5-7]. In the presence of target species, luminescence sensing techniques detect various analytes either through fluorescence quenching or enhancement of the signal, wavelength shift, and fluorescence intensity ratio (FIR) method. Several earlier reports of fluorescence-based amine sensors were mostly relied on single wavelength emitting organic semiconductor materials [8-10] metal organic framework materials [5,11-13], organic dyes [14], conjugated polymers [15], etc. In contrast to single emission FL detection, the dual emission probes have advantages of high accuracy and sensitivity as they recognize the analyte by utilizing the ratio between the two emission centers at distinct wavelengths as analytical signal, while simultaneously cancelling out the background factors that originates from concentration, environment, and excitation intensity. Additionally, a visual color change is possible in such cases which help onsite detection of the analytes which in turn triggers different fluorescence colors [16,17].

Halide based perovskite materials are currently at the leading edge of research as a potential candidate for photovoltaics and optoelectronic materials [18,19]. In contrast to typical luminous nanomaterials, inorganic metal halide perovskite nanomaterials possess advantageous optical properties and recently $CsPbBr_3$ perovskites have been explored in the area of various luminescence based sensing [20-24]. During the last few years, a range of gases or vapors including NH_3 [25,26], SO_2 [27], H_2S [28], O_2 [29], HCl [30], H_2O [31] and volatile organic chemicals have been identified by employing perovskite as fluorescent sensors. Wu et al. and kim et al. introduced $CH_3NH_3PbBr_3$ perovskite nanomaterials for the sensing of various volatile organic amines using fluorescence quenching process. After being subjected to amine vapor, the authors observed a color change of the perovskite film [3,32].

Considering the above discussion, this chapter emphasized the preparation of a stable dual emitting probe sensor by combining $CsPbBr_3$ with luminescent Eu-BDC matrix. The proposed sensor can act as a ratiometric probe for volatile aliphatic amine detection, where $CsPbBr_3$ signal display a photoluminescence (PL) enhancement response while Eu-BDC serves as a standard signal to build a self-calibration system. Most of the previous literatures of amine sensing using perovskites were based on PL quenching mode. This dual mode ratiometric turn on sensing probe demonstrates significantly improved selectivity and sensitivity compared to earlier reports that typically apply thin films of polycrystalline or single crystals of perovskites. Additionally, the sensor's functionality for real-time meat freshness monitoring was verified.

5.2. Experimental

5.2.1. Materials

The reagents used in this work were obtained from commercial suppliers and used without any further purification. Cesium bromide (CsBr, 99.9%, alfa aesar^R), lead bromide ($PbBr_2$, 99.9%, alfa aesar^R), oleic acid (OA, 90%, alfa aesar^R), oleylamine (OAm, 99%, alfa aesar^R), europium chloride hexahydrate ($EuCl_3.6H_2O$, 99%, alfa aesar^R), 1,4-benzene dicarboxylic acid (BDC, alfa aesar^R), 1,10-phenanthroline (Sigma Aldrich), Sodium hydroxide (NaOH, SRL^R Chemical), N, N-dimethylformamide (DMF, 99%, Merck^R), toluene (C_7H_8, Merck^R), ultrapure water.

5.2.2. Methods

5.2.2.1. Synthesis of Eu-BDC

Eu-BDC was synthesized following a previous literature [33] using hydrothermal route. In a mixture 0.2475 g of $EuCl_3.6H_2O$, 0.1886 g of BDC, 0.133 g of 1,10-phenanthroline, and NaOH solution (0.65 M in 2 ml water) were dissolved in 20 ml of water. Then the mixture was moved into a 100 ml Teflon lined autoclave and heated at 170°C for 48 h. After that, the mixture was slowly cooled to room temperature. Then, the obtained white products were washed several times with water/ethanol mixture, and separated by centrifugation. Finally, the Eu-BDC crystals were obtained by vacuum drying the white solids at 80°C for 4 hours.

5.2.2.2. Synthesis of $CsPbBr_3$/Eu-BDC composite

To synthesize $CsPbBr_3$/Eu-BDC composite, 100 mg of as prepared Eu-BDC was dispersed in 10 ml DMF. Separately a 0.5 mmol of $PbBr_2$ and CsBr was added in 5 ml DMF with 0.12 ml of OA and 0.03 ml of OAm. The mixture was stirred for 15 min to form a clear precursor. The precursor mixture was then gradually added into the Eu-BDC dispersion in DMF and stirred for one hour. Then the supernatant solutions were discarded and 10 ml toluene was poured into the mixture to induce the crystallization of $CsPbBr_3$ perovskites in the Eu-BDC matrix. The stirring was continued for another 2 h. The obtained solids were then separated by filtration and dried at 70°C for four hours.

5.2.2.3. Preparation of samples for fluorescence measurement

For liquid phase detection of amines, a 5 ml of 2 mg ml^{-1} homogeneous composite dispersion in hexane was served as the standard and the emission intensity of 3 ml standard was measured using a $1cm^3$ quartz cuvette. Thereafter, 100 µl of various aliphatic amines of different concentrations were subsequently added to $CsPbBr_3$/Eu-BDC dispersion for sensing experiment and incubating at room temperature for 10 sec. Fluorescence spectra of the as prepared solutions were recorded at an excitation wavelength of 330 nm. For vapor phase identification, the probe composite loaded paper substrate was prepared using the method described in the earlier chapter (Chapter 3, section 3.2.2.4). After suspended over the saturated amine vapor solution, the solid-state PL measurements were performed.

5.2.2.4. Real sample evaluation with raw meat product

We procured raw meat from local market of napaam, Tezpur. To get the released amine vapor from meat samples two fresh chicken meat pieces (of weight1g) were taken and separately kept inside a sealed beaker. One of them was stored at 4℃ (refrigerator) and the other was placed at normal room temperature (25℃). The paper strip (1 cm ×1 cm) with the loaded sample was then placed over the meat containing beaker and the luminescent measurements of the samples were performed over different duration of time to monitor the changes in the FL intensity.

5.2.2.5. Characterization methods

Fourier transform infrared (FTIR), X-ray diffraction patterns (XRD), X-ray photoelectron spectroscopy (XPS), energy dispersive X-ray spectroscopy (EDX) analyses were used for the structural and elemental characterization of the samples. Morphological characterizations were conducted in scanning electron microscope (SEM) and transmission electron microscope (TEM). UV-Vis absorption spectra, PL emission spectroscopy, and Time-resolved PL decay measurements were carried out to study the optical properties. Instruments used for these characterizations are described in previous chapter.

5.3. Results and Discussion

Eu-BDC matrix was synthesized by following a hydrothermal method in which $EuCl_3.6H_2O$ reacted with the linker benzene dicarboxylic acid. After addressing $CsPbBr_3$ PeNCs via a one pot synthetic method to the Eu-BDC, the white solid transform into yellow colored solid. The synthesized samples were then analyzed with various analytical tools.

5.3.1. Structural and elemental characterization of $CsPbBr_3$/Eu-BDC

5.3.1.1. FTIR analysis

For surface functional group analysis of the synthesized samples, FTIR spectra were recorded. Figure 5.1 displayed the FTIR spectra of Eu-BDC and $CsPbBr_3$/Eu-BDC composite. The parent Eu-BDC's carboxylate group showed the typical peaks for symmetric and asymmetric stretching vibration at 1396 $cm^{-1}$and 1640 cm^{-1}, respectively, showing the coordination of carboxylate group in the ligand to europium ions. The peak

at 3495 cm^{-1} is ascribed to the coordinated H_2O with the metal ion. The vibrational band in the region of 740-850 cm^{-1} corresponds to the bending vibration of benzene ring. The metal oxygen bond of Eu-BDC assigned a peak at around 515 cm^{-1}. The FTIR spectrum of $CsPbBr_3$/Eu-BDC composite possessed the distinctive absorption bands of Eu-BDC indicating the successful formation of the composite. The peaks at 2923 cm^{-1} and 2854 cm^{-1} are ascribed to the asymmetrical and symmetrical stretching vibration of C-H.

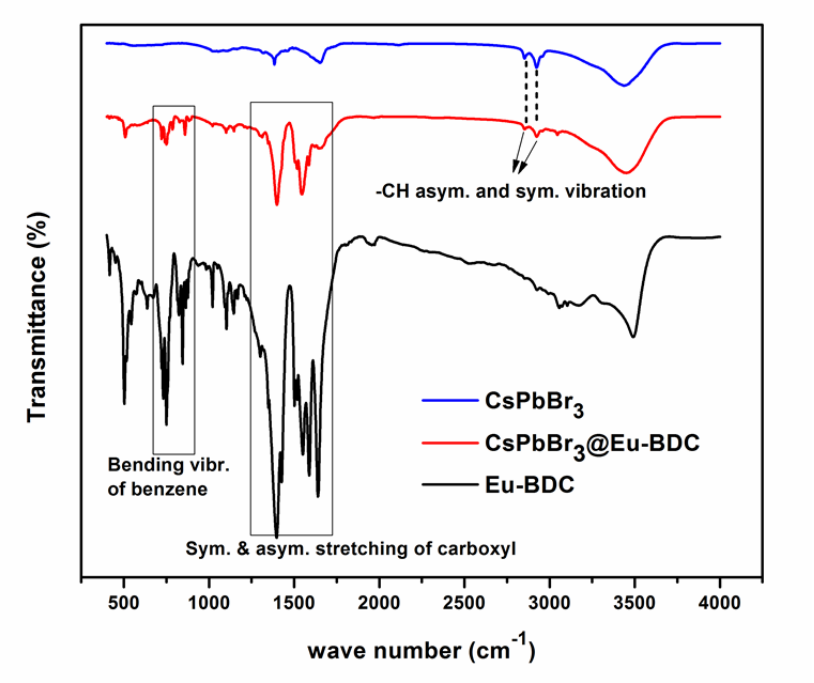

Figure 5.1: FTIR spectra of bare Eu-BDC, $CsPbBr_3$, and $CsPbBr_3$/Eu-BDC .

5.3.1.2. XRD analysis

Figure 5.2 depicted the recorded PXRD pattern of Eu-BDC and $CsPbBr_3$/Eu-BDC. Eu-BDC shows typical XRD peaks at about 2θ value 9.49°, 10.09°, 11.58°, 13.15°, 20.28°, and 29.12° assigning to the (010), (110), (111), (101), (220), and (222) planes (CCDC: 222296) [34]. Characteristic diffraction peaks of Eu-BDC are clearly discernible in the $CsPbBr_3$/Eu-BDC composite, demonstrating that the framework is preserved during the formation of the composite. Three new sharp peaks at 2θ around 34.4°, 37.8° and 43.7° were observed which are assigned to the (210), (211), and (220) planes of $CsPbBr_3$ perovskites [35].

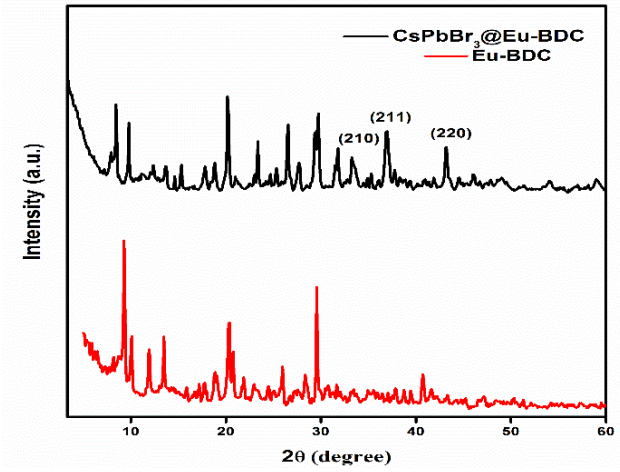

Figure 5.2 XRD pattern of bare Eu-BDC (red) and $CsPbBr_3$/Eu-BDC (black).

5.3.1.3. Energy Dispersive X-ray Analysis (EDX)

EDX spectrum in Figure 5.3a displays the existence of Eu, C, O of Eu-BDC MOF. In the EDX spectrum of $CsPbBr_3$/Eu-BDC (Figure 5.3b), signals of Cs, Pb, Br and Eu, C, O are observed, specifies the formation of $CsPbBr_3$/Eu-BDC composite. The corresponding elemental mappings of Cs, Pb and Br obtained from the composite (Figure 5.3c) reveal the uniform distribution of the $CsPbBr_3$ component elements in the Eu-BDC matrix.

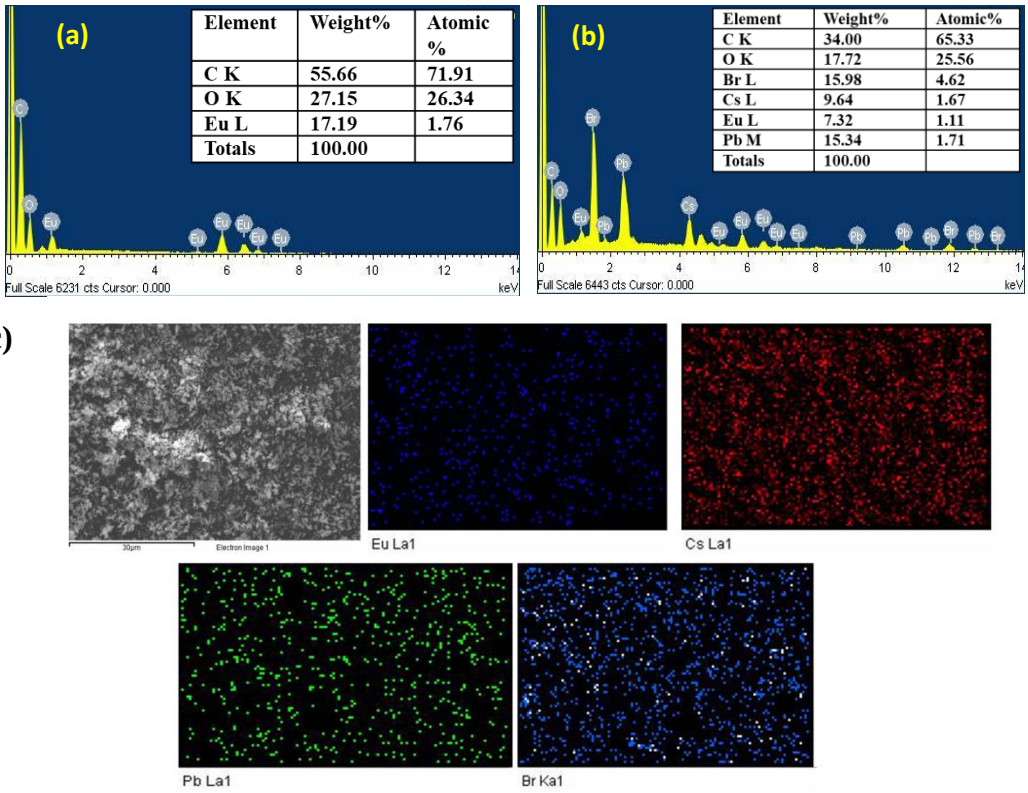

Figure 5.3: EDX spectra of Eu-BDC (a), and $CsPbBr_3$/Eu-BDC (b), EDX mapping images of Cs, Pb, Br, and Eu elements of $CsPbBr_3$/Eu-BDC (c).

5.3.1.4. X-ray Photoelectron spectroscopy analysis

XPS analysis of the synthesized $CsPbBr_3$/Eu-BDC was performed to know the surface chemical interaction of $CsPbBr_3$ and Eu-BDC. The survey XPS spectrum (Figure 5.4a) revealed the presence of the corresponding peaks of component elements (Cs, Pb, Br, Eu, C, N, and O) from both Eu-BDC and $CsPbBr_3$ NCs, assigning the formation of the composite. The core level XPS spectra of Cs 3d (Figure 5.4b) and Pb 4f (Figure 5.4c) revealed two characteristic peaks of Cs $3d_{5/2}$ (723.38 eV), Cs $3d_{3/2}$ (737.5 eV) and Pb $4f_{5/2}$ (141.8 eV), Pb $4f_{7/2}$ (136.9 eV) respectively. Br 3d XPS spectrum showed Br $3d_{5/2}$ peak at 67.1 eV and Br $3d_{3/2}$ at 67.9 eV (Figure 5.4d). Also, Eu *3d* spectrum revealed two peaks corresponding to Eu $3d_{5/2}$ (1133.6 eV) and Eu $3d_{3/2}$ (1153.5 eV) states from Eu-BDC. Figure 5.5a and 5.5b showed C *1s*, and O *1s* band of $CsPbBr_3$/Eu-BDC composite. C *1s* core spectrum could be divided into three peaks at 284.5 eV (C=C/ C-H), 285.2 eV (C-N), and 288.5 eV (COO^-), mainly contributed from BDC ligand. The lower binding energy levels of O*1s* (Figure 5.5b) appeared at 529.3 eV and 529.9 eV attributed to the presence of metal oxygen coordinate bond, indicating a close interaction of $CsPbBr_3$ and Eu-BDC. The high energy peak of O*1s* centered at 531 eV referred to –C=O group of BDC ligand. The XPS result further validates the successful formation of the composite.

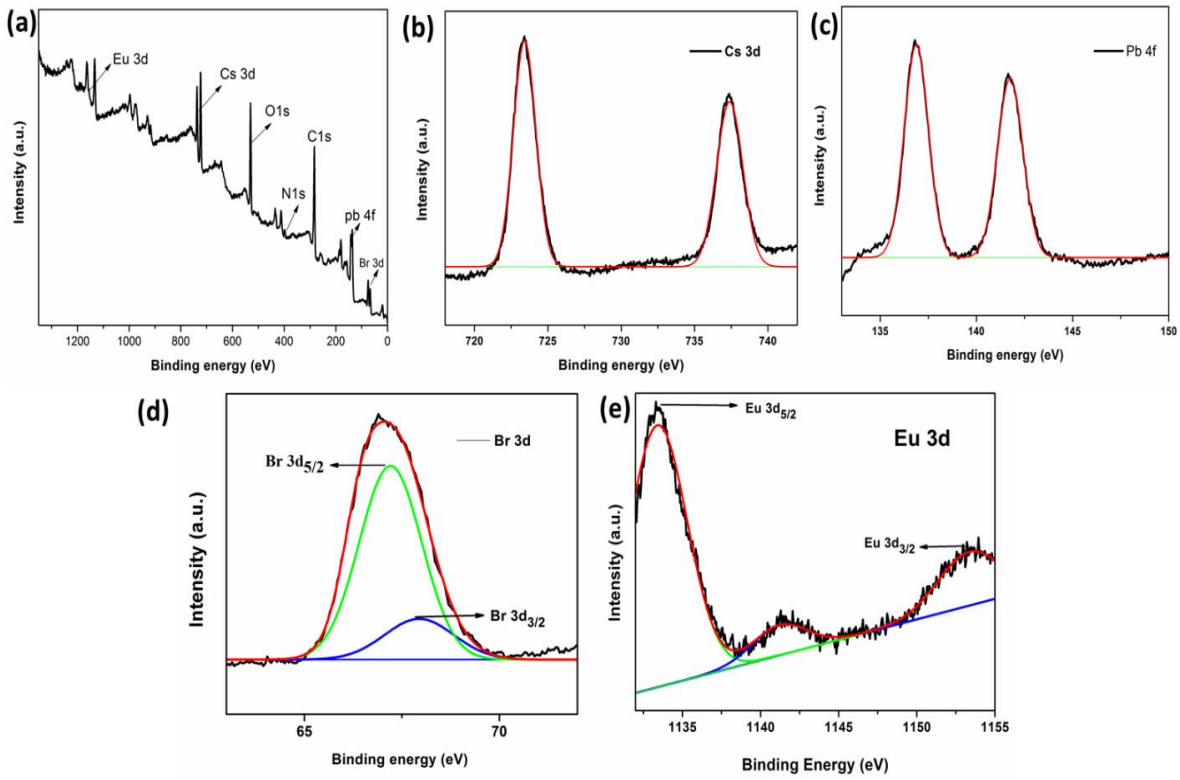

Figure 5.4: XPS survey profile of $CsPbBr_3$/Eu-BDC (a), core level XPS spectra of Cs *3d* (b), Pb *4f* (c), Br *3d* (d), and Eu *3d* (e).

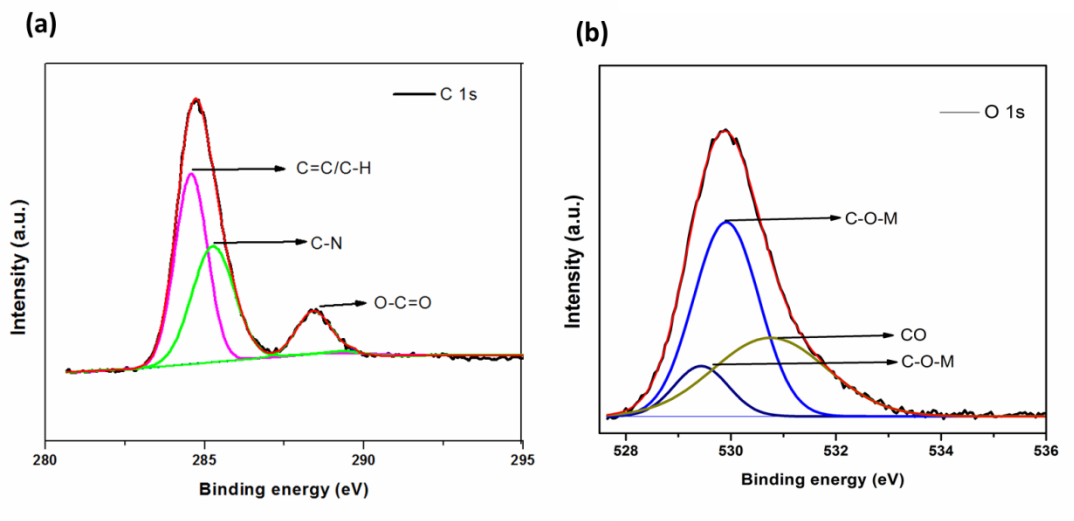

Figure 5.5: XPS fine spectra of C*1s* (a) and O*1s* of $CsPbBr_3$/Eu-BDC nano composite.

5.3.2. Morphological analysis

5.3.2.1. SEM analysis

As revealed from the SEM images in Figure 5.6a, the Eu-BDC has regular rhomboid shape morphology. Additionally, $CsPbBr_3$/Eu-BDC composites did not significantly change the size or morphology of Eu-BDC which was displayed in Figure 5.6b.

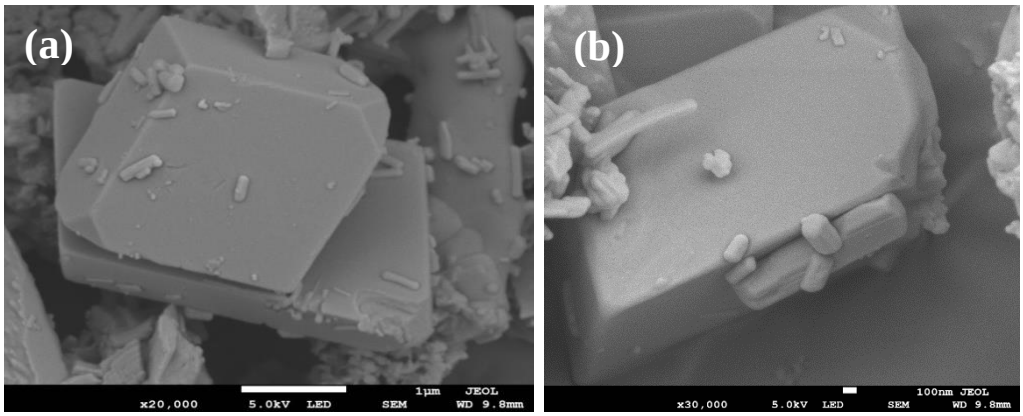

Figure 5.6: SEM micrograph images of Eu-BDC (a) and $CsPbBr_3$/Eu-BDC (b).

5.3.2.2. TEM analysis

The nanoscale composite morphology and crystal size was then characterized with TEM imaging analysis. $CsPbBr_3$ particles were shown to be encased in Eu-BDC matrix (Figure 5.7a). The well-defined lattice fringes were observed in the HRTEM image (Figure 5.7b) with a fringe spacing value of 0.337 nm, which is in good agreement with the (111) plane of $CsPbBr_3$. These findings support the great crystallinity of the composite.

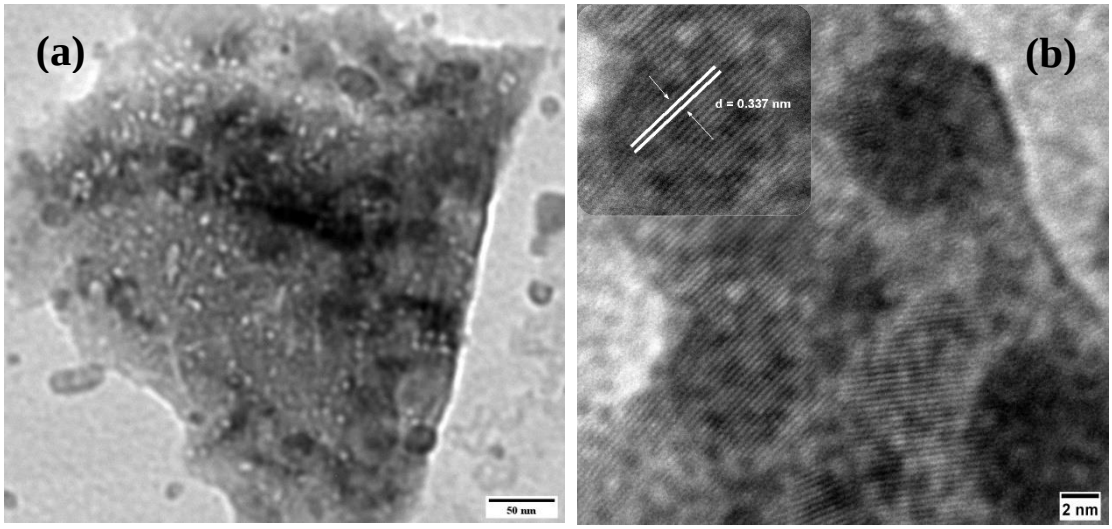

Figure 5.7: TEM image (a) and HRTEM image (b) of $CsPbBr_3$/Eu-BDC composite, inset shows the interplanar spacing of lattice fringes for (111) plane.

5.3.3. Optical property analysis of Eu-BDC and $CsPbBr_3$/Eu-BDC

To study the optical properties of the synthesized materials, absorption and emission spectra were recorded. Figure 5.8a shows that the distinctive absorption peaks at 245, 283, and 375 nm were visible in Eu-BDC. After incorporating $CsPbBr_3$ in Eu-BDC, the UV-Vis spectra of $CsPbBr_3$/Eu-BDC exhibited characteristics peaks located at 514, 250, and 365 nm. Following this, the emission properties of Eu-BDC MOF, and $CsPbBr_3$/Eu-BDC were examined. The luminescence spectra of Eu-BDC (Figure 5.9a) revealed the typical emission peaks centered at 592 and 615 nm, which were assigned for $5D_0 \rightarrow 7F_J$ (J = 1, 2) transition of Eu^{3+} ion [33]. Eu-BDC exhibits remarkable orange luminescence that can be visible with bare eyes under 330 nm UV light irradiation (inset photograph of Figure 5.9a). The emission of Eu-BDC with different excitation wavelength is presented in Figure 5.9b, which displayed variation in the intensity of Eu-BDC with excitation wavelength. With increase in excitation from 280 to 330 nm the emission intensity starts increasing, and then decreases with further increase in excitation wavelength. As depicted in Figure 5.8b, the emission peak of bare $CsPbBr_3$ perovskite was observed at 522 nm. Consequently, there were three distinct emission peaks visible in the $CsPbBr_3$/Eu-BDC composite material, located at 518 nm, 592 nm, and 615 nm, that are resulted from both the $CsPbBr_3$ perovskite and Eu-BDC emission centers respectively (Figure 5.8b). All the above discussed results established the successful formation of the dual emitting fluorescent composite. When compared to the luminescence from $CsPbBr_3$ PeQDs without

Eu-BDC, a negligible emission peak shifting ascribed to the similar emission behavior of $CsPbBr_3$ after introduced in the Eu-BDC matrix. Next, the PL spectra of $CsPbBr_3$/Eu-BDC composite were recorded with different excitation wavelength 330 – 365 nm (Figure 5.10). As the excitation wavelength increased the PL intensity at 518 nm associated with $CsPbBr_3$ was enhanced and that of the Eu-BDC PL intensity at 592 and 614 nm decreased. When the excitation wavelength was greater than 340 nm, hardly no fluorescence was detected for Eu-BDC. Therefore the optimized excitation wavelength for the sensing experiment was selected to be 330 nm.

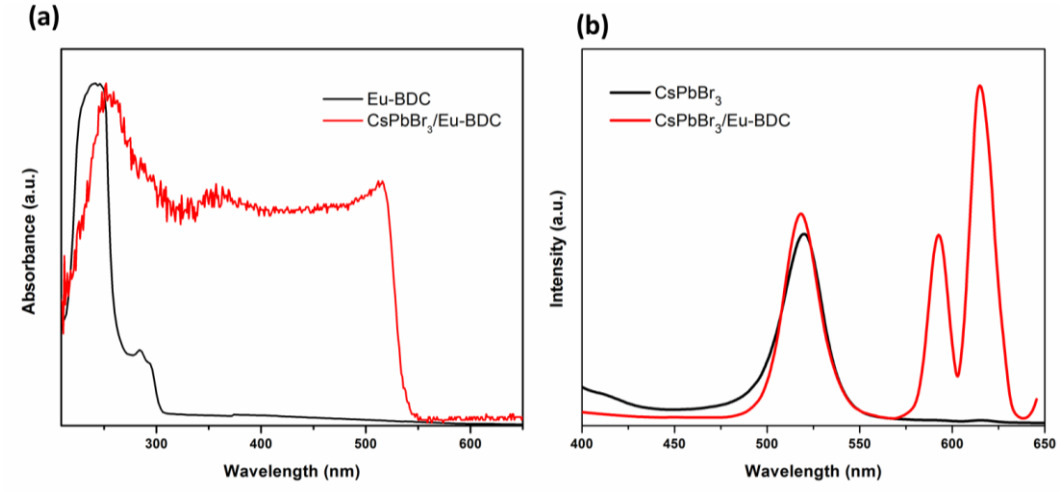

Figure 5.8: Absorption (a) spectra of Eu-BDC (black) and $CsPbBr_3$/Eu-BDC (red), Emission spectra (b) of $CsPbBr_3$ (black) and $CsPbBr_3$/Eu-BDC.

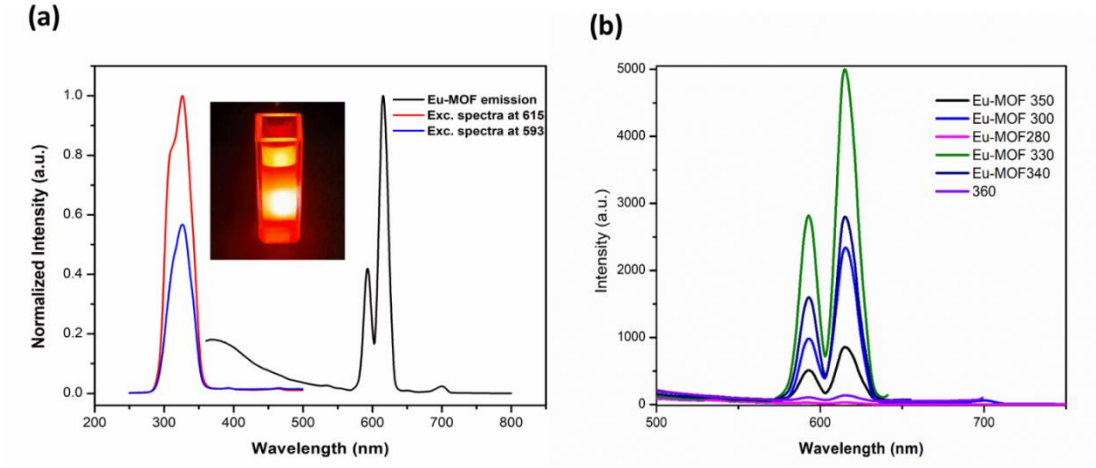

Figure 5.9: Excitation and emission spectra of Eu-BDC (a), emission spectra of Eu-BDC at different excitation wavelength (b).

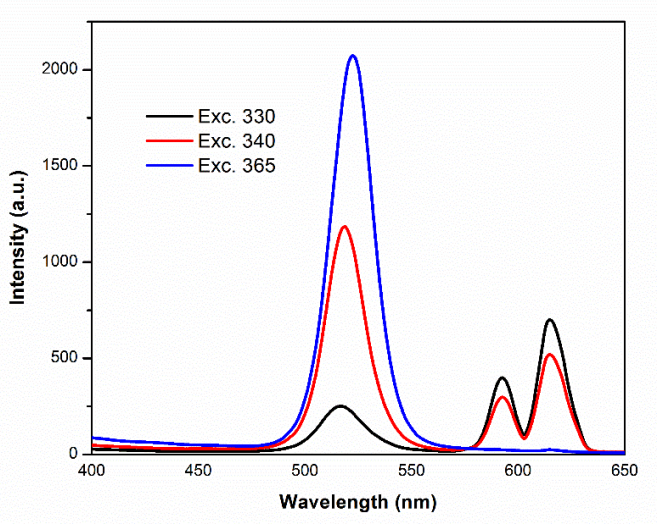

Figure 5.10: $CsPbBr_3$/Eu-BDC emission spectra at different excitation wavelength (330, 340, and 365 nm).

5.3.4. Analytical application of the composite

We then examined the sensing behavior of $CsPbBr_3$/Eu-BDC toward various volatile organic amine derivatives by checking the PL peak heights of $CsPbBr_3$ and Eu-BDC. The selected target analytes for this study includes methyl amine (MA), diethyl amine (DEA), triethyl amine (TEA), and ethylene diamine (EDA). Organic amines with primary aliphatic amine group showed the highest response to the photoluminescence of $CsPbBr_3$/Eu-BDC composite (Figure 5.11). As revealed from Figure 5.11, with the introduction of aliphatic amine solutions to the system, $CsPbBr_3$/Eu-BDC dispersion showed enhancement of the PL signal at 518 nm.

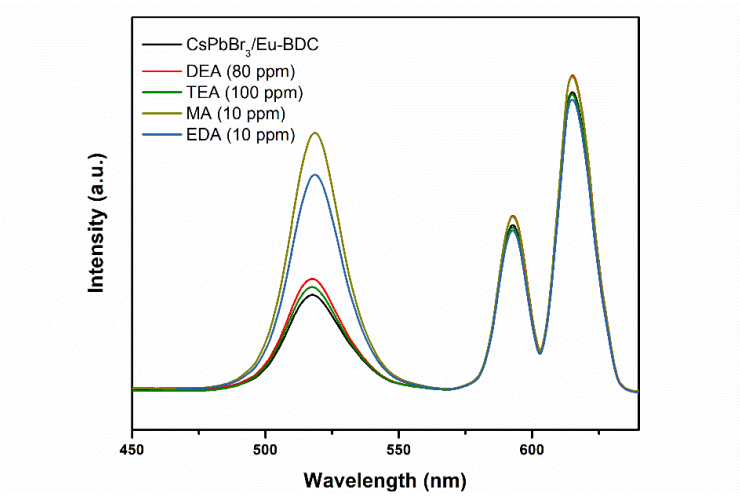

Figure 5.11: Emission spectra of $CsPbBr_3$/Eu-BDC with different aliphatic amines (concentration of the amines in ppm was indicated in parentheses).

5.3.4.1. Liquid phase detection of volatile organic amines: The quantitative response of methyl amine was studied with the incremental addition of different concentrations of methyl amine solution to the $CsPbBr_3$/Eu-BDC dispersed in hexane. Thereafter, the emission intensity of the probe was monitored at regular intervals, following each progressive addition of MA. $CsPbBr_3$/Eu-BDC sensor probe exhibited a fluorescence turn on behavior of the PL peak centered 518 nm whereas the emission at 615 nm showed negligible or little response to methyl amine addition (Figure 5.12a). Thus, we employed this designed sensor as ratiometric detection probe for methyl amine solution. Alongside, we observed a visual color change from red to green under UV light with the addition of methyl amine which was displayed in Figure 5.12c. The potential of the designed sensor was then verified by plotting the calibration curve between intensity ratios (I_{518}/I_{615}) and concentration of the analyte. The curve demonstrated a linear correlation within the range of methyl amine concentration (0-21) ppm having a R^2 value of 0.99227. The calculated detection limit was estimated to be 0.083 ppm for methyl amine using the relation 3σ/k [5], where k is slope of the curve and σ denotes standard deviation.

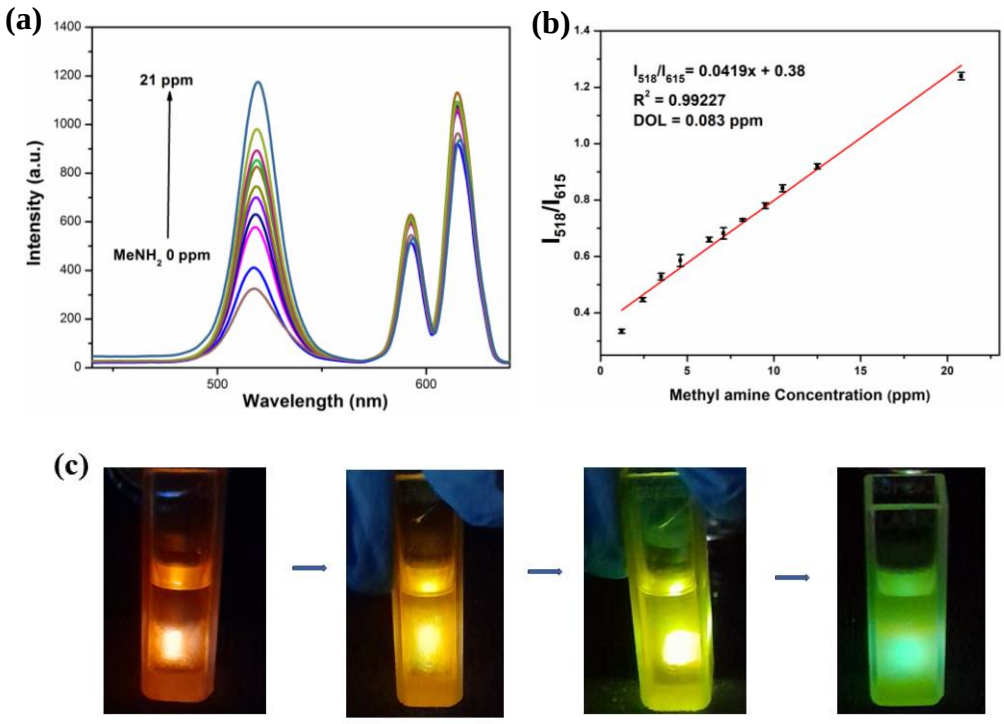

Figure 5.12: PL intensity graph of $CsPbBr_3$/Eu-BDC dispersion with the addition of MA (a), correlation graph of intensity ratio vs. concentration of MA (b), optical photograph showing the color change of the sensor with the subsequent addition of MA under UV lamp (c).

Table 5.1 Summary of various fluorometric sensors for aliphatic amines detection. (NM: Not mentioned)

Materials	Sensing Principle	Analytes	LOD	Application	Ref
Thiadiazole functionalized Zr(IV) MOF	FL enhancement	Aliphatic amines	66.2 nM Methyl amine (MA)	NA	[5]
Cationic covalent organic framework	FL enhancement	NH_3 and Primary amines	(0.002-0.004) ppm	Food spoilage	[11]
[Zn(PA)(BPE)] coordination polymer	FL enhancement	Aliphatic amines	9.9 ppm (EDA)	NA	[13]
Eu(III) tris-benzoylacetonate	Quenching	Methylamine	15.5 ppm	NA	[36]
$CH_3NH_3PbBr_3$ perovskite film	Quenching	($EtNH_2$, Et_2NH, Et_3N)	NM	NA	[3]
Fluorescent carbon nanotubes	Quenching	Aliphatic amines	NM	Meat spoilage	[10]
$CH_3NH_3PbBr_3$	Quenching	Aliphatic amines (DEA, TEA, PA, AN)	NM	NA	[32]
mp-TiO_2-$CH_3NH_3PbBr_3$	FL enhancement	NH_3 gas and Aliphatic amines	0.92 ppm (NH_3)	NA	[37]
$HPbBr_3/PbBr_2@SiO_2$	FL enhancement	Methyl amine	70 ppb	NA	[38]
CD/CdTe	Ratiometric	Biogenic Amines	0.168 ppm	Food samples	[39]
UCNP@mSiO_2@TDPM	Ratiometric	Biogenic Amines (spermine)	0.11µM	Fish and milk	[40]
Eu@Tt-TPA	Ratiometric	Methyl amine	0.87 ppm	Waste water	[41]
$CsPbBr_3$/Eu-BDC	Ratiometric	Aliphatic Primary amines	0.083 ppm (MA)	Meat spoilage	This work

Table 5.1 addressed the performance of the designed amine sensor with earlier reports of fluorescence materials and it reflects that our sensing probe gives a highly competitive result. This finding is indicative of a self-calibration phenomenon occurring in $CsPbBr_3$/Eu-BDC ratiometric sensor, which uses the reference Eu-BDC signal to suppress background noise.

Durability and photostability are two key metrics that show how well this PL sensor is performing, and these factors were investigated. For the quantitative study of sensing properties, we initially investigated the photo stability of $CsPbBr_3$/Eu-BDC composite at 518 nm by exposing it under 365 nm UV light for 40 h. From Figure 5.13a, the retained PL intensity of $CsPbBr_3$/Eu-BDC composite was found to be 66.67%. Only 33.3% of initial emission intensity of $CsPbBr_3$ was lost after 40 hours of exposure, presenting a stable sensing environment of the designed PL sensor. Later, the durability of $CsPbBr_3$/Eu-BDC in humid environment (~70% humidity) was examined for different interval of time within 25 hour by recording the emission spectra of the composite dispersion in hexane. Within a time frame of 25 hours, the $CsPbBr_3$/Eu-BDC intensity ratio (I_{518}/I_{615}) remained steady with no significant fluctuations. The respective results show that the developed sensor works reliably under ambient conditions.

For a better insight into the sensor's self-calibration behavior for amines, we observed the PL spectra of pristine $CsPbBr_3$ and Eu-BDC with varying concentrations of amines under the same experimental conditions.

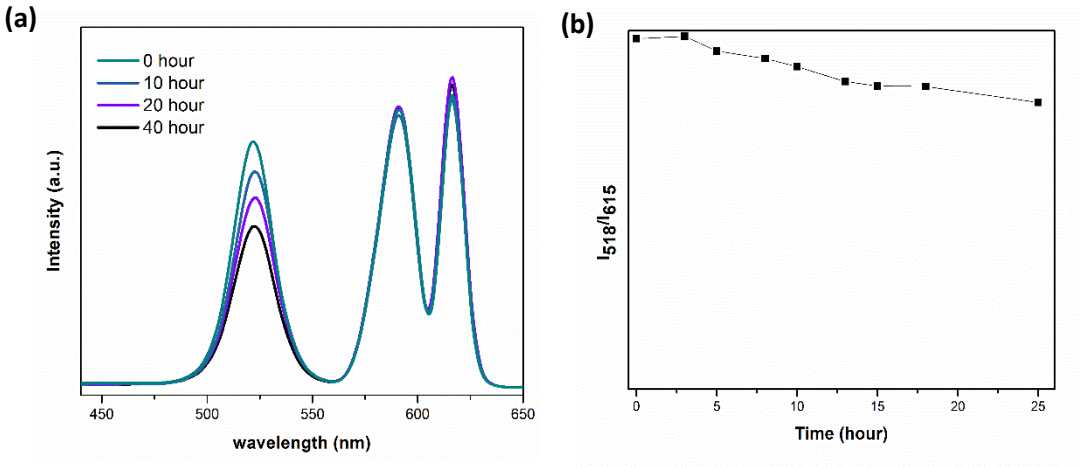

Figure 5.13: Photostability of $CsPbBr_3$/Eu-BDC under UV light for 40 h (a), humidity stability test of the sensor for 25 h.

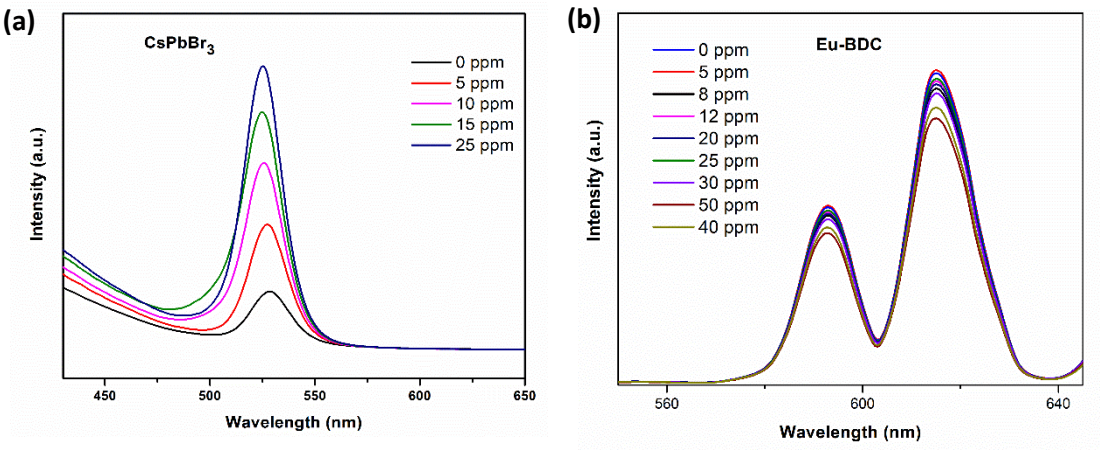

Figure 5.14 Emission spectra of pristine $CsPbBr_3$ (a) and Eu-BDC (b) with methyl amine.

Figure 5.14 reveals the rapid increase of the PL intensity of $CsPbBr_3$ with the introduction of amines, whereas the Eu-BDC showed a small change in intensity as the amine concentration was raised. This finding suggests that $CsPbBr_3$/Eu-BDC may have inherited its rapid amine response from the parent $CsPbBr_3$ perovskite.

Further, to gain deeper insights of the fluorescence turn on response with aliphatic amines, TRPL decay measurements were performed. Figure 5.15 displays the TRPL measurements of $CsPbBr_3$/Eu-BDC nanocomposite without or with the exposure of methylamine. At 518 nm emission, the composite showed a bi-exponential decay with the decay function- $Y = Y_0 + A_1 \exp(-x/\tau_1) + A_2 \exp(-x/\tau_2)$. Average life time of $CsPbBr_3$ of the composite was determined to be 21.40 ns, and with the addition of a little methylamine concentration 5 ppm and 20 ppm the life time enhances to 28.52 ns and 31.9 respectively. On the other hand, the FL lifetime for Eu-BDC signal at 615 nm barely changed (τ_{avg} = 3.01 ns without and 2.97 ns with MA) (Table 5.2). This outcome further validates the FL turn on phenomenon of the proposed sensor with methyl amine exposure which is ascribed to the reduction of defect levels of $CsPbBr_3$ with the treatment of methyl amine. Therefore, aliphatic amine treatment can reduce the nonradiative recombination of $CsPbBr_3$ perovskite, which in turn increases the PL intensity [35]. After introducing methyl amine, a negligible blue shift of about one nm in the sensor PL peak at 518 nm was noticed. Moreover, the UV-Vis absorption spectra (Figure 5.16a) of $CsPbBr_3$/Eu-BDC did not appear any new band. It indicates that the composite's crystal size and shape are unchanged. To understand the structural evolution of the composite following methyl amine treatment, XRD diffraction analysis was performed. As observed in Figure 5.16b,

the typical diffraction peaks of $CsPbBr_3$/Eu-BDC with methylamine are identical to those of pristine one.

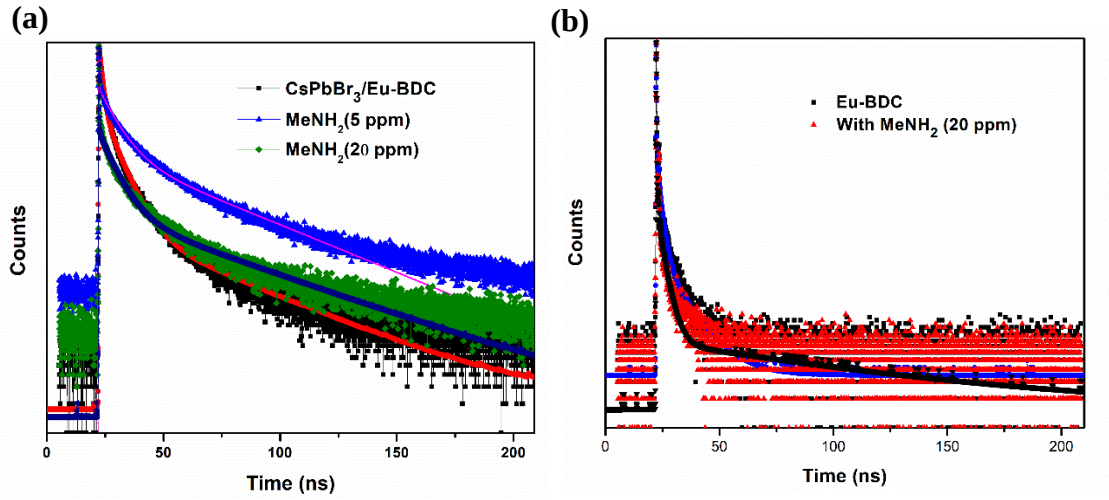

Figure 5.15: TRPL decay curves of $CsPbBr_3$/Eu-BDC (a) and Eu-BDC (b) without or with the treatment of methyl amine.

Table 5.2. Life time values from TRPL analysis

Samples	**τ_1 (ns)**	**τ_2 (ns)**	**τ_3 (ns)**	**τ_{avg} (ns)**
$CsPbBr_3$/Eu-BDC	4.68	29.37	0.899	21.4
$CsPbBr_3$/Eu-BDC (with 5 ppm CH_3NH_2)	5.02	30.69	0.066	28.52
$CsPbBr_3$/Eu-BDC (with 20 ppm CH_3NH_2)	4.65	34.93	0.041	31.9

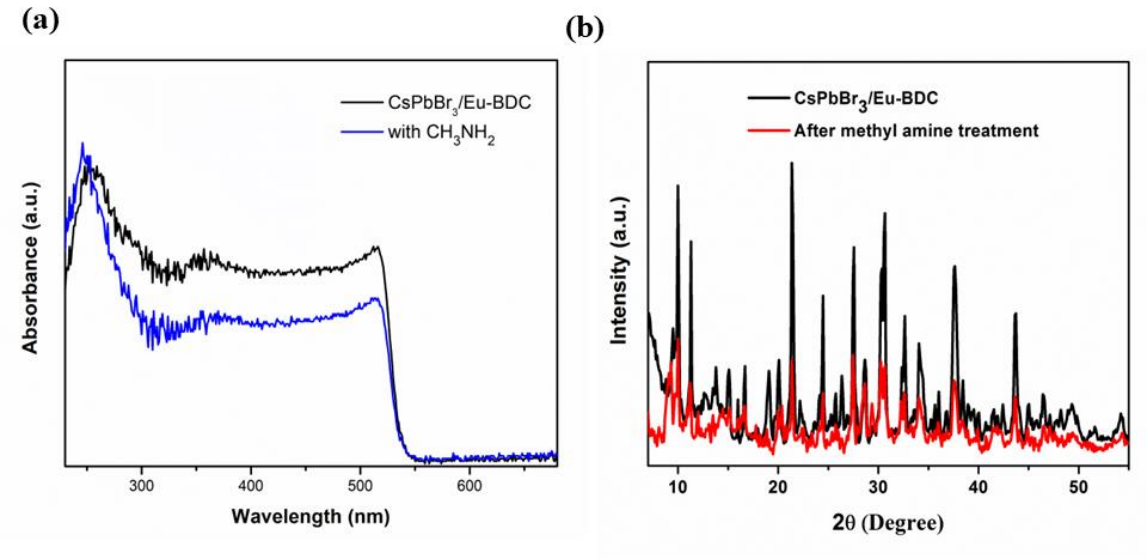

Figure 5.16: Absorption spectra (a) and PXRD patterns (b) of $CsPbBr_3$/Eu-BDC on exposure with MA.

5.3.4.2 Selectivity investigation

The impacts of commonly used organic solvents, as indicated in Figure 5.17 on ratiometric luminescence response of the composite were studied under similar experimental conditions. FL responses to these solvents (Ethanol, Methanol, Acetone, DMF, THF, DCM, Benzene, Toluene, Hexane, Water) are extremely low, and as expected the designed $CsPbBr_3$/Eu-BDC dual sensor exhibited selective turn on response for only aliphatic amines. A little bit decrease in PL intensity of the composite was occurred when aromatic amines (aniline) were present. Among the selected aliphatic amines including methyl amine (MA), ethylene diamine (EDA), cadaverine, putrescine, diethyl amine (DEA), and triethyl amine (TEA), it is to be noted that there is some variation in ratiometric amine sensing. The highest ratiometric response was observed for methyl amine. Similarly, EDA, cadaverine, and putrescine also resulted in significant quantitative PL response. Bulky aliphatic amines, diethyl amine (DEA) and triethyl amine (TEA) showed very low response. More than two to three-fold enhancement in ratiometric response was noticed in case of primary aliphatic amines (MA, EDA, cadaverine, putrescine). Steric hindrance may contribute for such observations [11]. From these findings, it seems reasonable to conclude that our sensor has good sensitivity and selectivity for aliphatic primary amines and remains unaffected by other organic solvents.

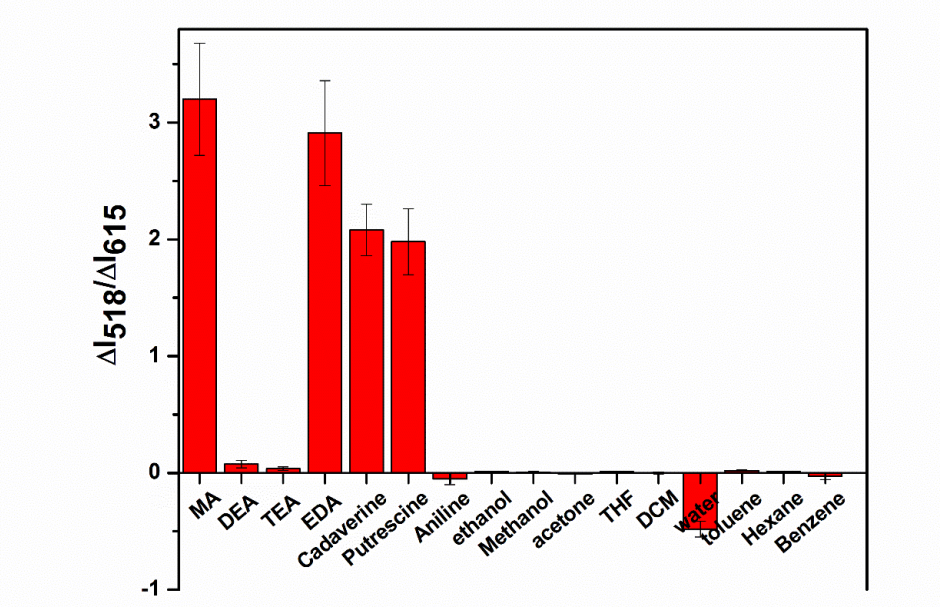

Figure 5.17: Bar graph representing the PL ratiometric response of the sensor with various organic amines and organic solvents.

5.3.5 Vapor phase identification of amines

To increase the practical utility of the designed sensor, the vapor phase sensing ability of amines was also carried out. The sealed beakers with various aliphatic amine solution were kept for three hours to obtain the saturated vapors of the corresponding amine solutions. Thereafter the perovskite composite loaded test paper film was suspended over the saturated vapors at room temperature and the emission spectra of the sample was analyzed. Figure 5.18 demonstrates the emission measurements of the sensor with different saturated amine vapors, which imply that the sensor can detect the presence of amine in vapor phase also. Similar PL response with solution phase amine can be observed in vapor phase also, with primary aliphatic amines exhibiting greater PL amplification than other amines.

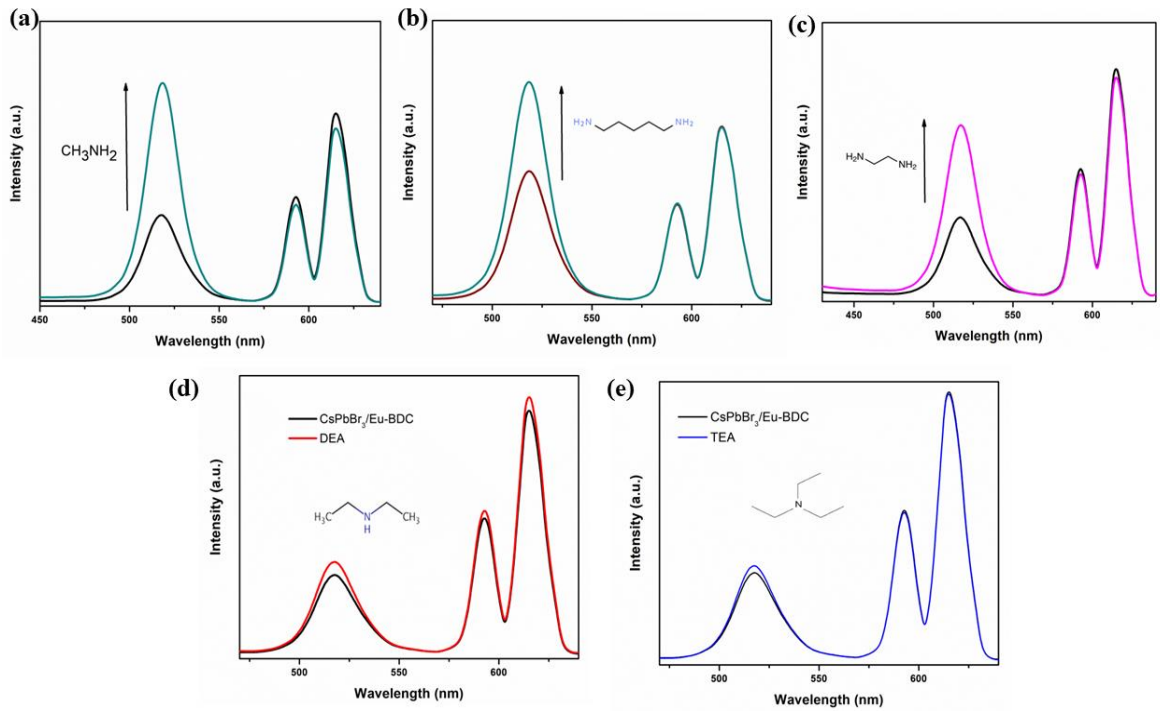

Figure 5.18: Fluorescence response of $CsPbBr_3$/Eu-BDC composite to methyl amine (a), cadaverine (b), ethylene diamine (c), diethyl amine (c), triethyl amine (e) saturated vapor exposure.

5.3.6 Application of the sensor in meat freshness detection

As we discussed earlier, the designed sensor gives extremely rapid response to the amine derivatives with primary aliphatic amine groups. It is highly sensitive to aliphatic diamines such as ethylene diamine. Therefore, we further studied the biogenic amines e.g., cadaverine and putrescine responses on PL intensity of $CsPbBr_3$/Eu-BDC and the sensor have very high sensitivity towards biogenic amines also (Figure 5.17). Since spoiled meat proteins releases various amines and biogenic amines like cadaverine, their detection is crucial for assessing the quality of meat products while they are being transported and stored. Consequently, we employed this sensor for the purpose of monitoring the emissions of amines from meat products. To get the released amine vapor from meat samples two fresh chicken meat pieces (of weight1g) were taken and separately kept inside a sealed beaker. One of them was stored at 4°C (refrigerator) and the other was placed at normal room temperature (RT). Luminescent measurements of the solid state samples were performed over different duration of time to monitor the changes in the FL intensity. After 48 h of storage time, the emission intensity of the sample at room temperature significantly increased by 47.4 %. On the other hand, comparatively less PL response (only 10 %) was

monitored for the sample kept inside the refrigerator due to the less emission of amine vapor (Figure 5.19). For the sample kept at RT, the disintegration of the sample starts at about 2 hours. Biogenic amine releases from the decaying meat sample stored at room temperature which in turn increase the PL intensity of the sensor at 518 nm. Thus, the designed dual emitting sensor can serve as a marker for determining the freshness of meat protein.

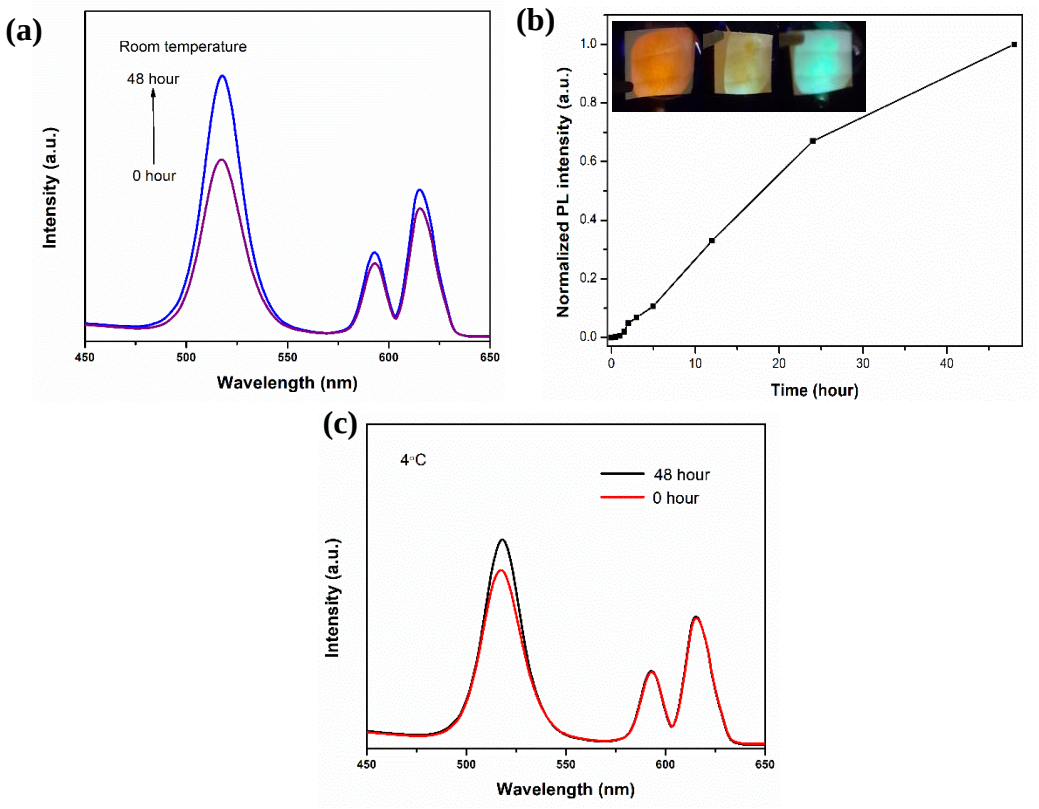

Figure 5.19: FL intensity measurements of the sensor probe upon exposure over chicken meat samples at room temperature (a) and at 4°C (c), Intensity vs. time graph for the meat sample stored at room temperature, inset: the photograph of probe coated test strips under UV light with (0 h, 24 h, 48 h) time in presence of rotten chicken flesh (b).

5.4. Conclusion

- ✓ This study demonstrates construction of a new ratiometric fluorescence sensor based on Eu-BDC MOF supported $CsPbBr_3$ perovskite for the selective recognition of primary aliphatic amines.
- ✓ In presence of amines the selected $CsPbBr_3$/Eu-BDC sensor exhibited an enhancement of the PL signal of $CsPbBr_3$ at 518 nm and the Eu-BDC signal at 615 nm served as a standard to construct the ratiometric sensing system.

- ✓ A visual color change from red to green was further observed with the incremental addition of methyl amine to the probe. An ultralow detection limit of 0.083 ppm was determined for methyl amine.
- ✓ This ratiometric sensor have very rapid and high fluorescence response to various primary aliphatic amines in both solution and vapor phase.
- ✓ It has been established that the sensor is effective at keeping track of the freshness of meat items that emit amine vapors when they decay.

5.5. References

[1] Ly, N. H., Kim, H. H., and Joo, S. W. On-Site Detection for Hazardous Materials in Chemical Accidents. *Bulletin of the Korean Chemical Society*, 42(1):4-16, 2021.

[2] Gao, T., Tillman, E. S., and Lewis, N. S. Detection and classification of volatile organic amines and carboxylic acids using arrays of carbon black-dendrimer composite vapor detectors. *Chemistry of materials*, 17(11):2904-2911, 2005.

[3] Kim, S. H., Kirakosyan, A., Choi, J., and Kim, J. H. Detection of volatile organic compounds (VOCs), aliphatic amines, using highly fluorescent organic-inorganic hybrid perovskite nanoparticles. *Dyes and Pigments*, 147:1-5, 2017.

[4] Park, B., Kim, S., Kwak, C. H., Shanmugam, K. R., Han, Y. K., Cho, Y., and Huh, Y. S. Visual colorimetric detection of ammonia under gaseous and aqueous state: Approach on cesium lead bromide perovskite-loaded porous electrospun nanofibers. *Journal of Industrial and Engineering Chemistry*, 97:515-522, 2021.

[5] Mallick, A., El-Zohry, A. M., Shekhah, O., Yin, J., Jia, J., Aggarwal, H., Emwas, A. H., Mohammed, O. F., and Eddaoudi, M. Unprecedented ultralow detection limit of amines using a thiadiazole-functionalized Zr (IV)-based metal–organic framework. *Journal of the American Chemical Society*, 141(18):7245-7249, 2019.

[6] Singh, A., Qu, Z., Sharma, A., Singh, M., Tse, B., Ostrikov, K., Popat, A., Sonar, P., and Kumeria, T. Ultra-bright green carbon dots with excitation-independent fluorescence for bioimaging. *Journal of Nanostructure in Chemistry*, 13(3):377-387, 2023.

[7] Kumar, R., Sharma, A., Singh, H., Suating, P., Kim, H. S., Sunwoo, K., Shim, I., Gibb, B. C. and Kim, J. S. Revisiting fluorescent calixarenes: from molecular sensors to smart materials. *Chemical reviews*, 119(16):9657-9721, 2019.

[8] Che, Y., Yang, X., Loser, S., and Zang, L. Expedient vapor probing of organic amines using fluorescent nanofibers fabricated from an n-type organic semiconductor. *Nano letters*, 8(8): 2219-2223, 2008.

[9] Che, Y. and Zang, L. Enhanced fluorescence sensing of amine vapor based on ultrathin nanofibers. *Chemical communications*, 34:5106-5108, 2009.

[10] Hu, Y., Ma, X., Zhang, Y., Che, Y., and Zhao, J. Detection of amines with fluorescent nanotubes: applications in the assessment of meat spoilage. *Acs Sensors*, 1(1):22-25, 2016.

[11] Das, G., Garai, B., Prakasam, T., Benyettou, F., Varghese, S., Sharma, S. K., Gándara, F., Pasricha, R., Baias, M., Jagannathan, R., and Saleh, N. I. Fluorescence turn on amine detection in a cationic covalent organic framework. *Nature communications*, 13(1):3904, 2022.

[12] Wang, F., Dong, C., Wang, C., Yu, Z., Guo, S., Wang, Z., Zhao, Y., and Li, G. Fluorescence detection of aromatic amines and photocatalytic degradation of rhodamine B under UV light irradiation by luminescent metal–organic frameworks. *New Journal of Chemistry*, 39(6):4437-4444, 2015.

[13] Mani, P., Ojha, A. A., Reddy, V. S., and Mandal, S. "Turn-on" fluorescence sensing and discriminative detection of aliphatic amines using a 5-fold-interpenetrated coordination polymer. *Inorganic Chemistry*, 56(12):6772-6775, 2017.

[14] Li, Z., Gao, X., Hu, X., Zhang, X., Jia, C., Liu, C., Shen, L., Zhu, H., Cui, M., Lu, Z., and Guo, H. Dithienylethenes functionalized by triphenylethene and difluoroboron β-diketonate fragments: synthesis, optical switching behavior and fluorescent turn-on sensing for volatile organic amines. *Dyes and Pigments*, 192:109422, 2021.

[15] Pavase, T. R., Lin, H., Hussain, S., Li, Z., Ahmed, I., Lv, L., Sun, L., Shah, S. B. H., and Kalhoro, M.T. Recent advances of conjugated polymer (CP) nanocomposite-based chemical sensors and their applications in food spoilage detection: A comprehensive review. *Sensors and Actuators B: Chemical*, 273:1113-1138, 2018.

[16] Shu, Y., Ye, Q., Dai, T., Guan, J., Ji, Z., Xu, Q., and Hu, X. Incorporation of perovskite nanocrystals into lanthanide metal-organic frameworks with enhanced stability for ratiometric and visual sensing of mercury in aqueous solution. *Journal of Hazardous Materials*, 430: 128360, 2022.

[17] Liu, J., Zhao, Y., Li, X., Wu, J., Han, Y., Zhang, X., and Xu, Y. Dual-emissive CsPbBr3@ Eu-BTC composite for self-calibrating temperature sensing application. *Crystal Growth & Design*, 20(1):454-459, 2019.

[18] Misra, R. K., Cohen, B. E., Iagher, L., and Etgar, L. Low-dimensional organic–inorganic halide perovskite: structure, properties, and applications. *ChemSusChem*, 10(19):3712-3721, 2017.

[19] Liu, P., Chen, W., Wang, W., Xu, B., Wu, D., Hao, J., Cao, W., Fang, F., Li, Y., and Zeng, Y. Halide-rich synthesized cesium lead bromide perovskite nanocrystals for light emitting diodes with improved performance. *Chemistry of Materials*, 29(12):5168-5173, 2017.

[20] Aldakov, D. and Reiss, P. Safer-by-design fluorescent nanocrystals: Metal halide perovskites vs semiconductor quantum dots. *The Journal of Physical Chemistry C*, 123(20):12527-12541, 2019.

[21] Wang, T., Wei, X., Zong, Y., Zhang, S., and Guan, W. An efficient and stable fluorescent sensor based on APTES-functionalized $CsPbBr_3$ perovskite quantum dots for ultrasensitive tetracycline detection in ethanol. *Journal of Materials Chemistry C*, 8(35):12196-12203, 2020.

[22] Guan, J., Shen, Y. Z., Shu, Y., Jin, D., Xu, Q., and Hu, X. Y. Internal–external stabilization strategies enable ultrastable and highly luminescent CsPbBr3 perovskite nanocrystals for aqueous Fe3+ detection and information encryption. *Advanced Materials Interfaces*, 8(19):2100588, 2021.

[23] Perveen, A., Hussain, S., Xu, Y., Raza, A., Saeed, F., Din, N., Subramanian, A., Khan, Q., and Lei, W. Solution processed and highly efficient UV-photodetector based on CsPbBr3 perovskite-polymer composite film. *Journal of Photochemistry and Photobiology A: Chemistry*, 426:113764, 2022.

[24] Muthu, C., Nagamma, S. R., and Nair, V. C. Luminescent hybrid perovskite nanoparticles as a new platform for selective detection of 2, 4, 6-trinitrophenol. *RSC advances*, 4(99):55908-55911, 2014.

[25] He, X., Yu, C., Yu, M., Lin, J., Li, Q., Fang, Y., Liu, Z., Xue, Y., Huang, Y., and Tang, C. Synthesis of perovskite CsPbBr3 quantum dots/porous boron nitride nanofiber composites with improved stability and their reversible optical response to ammonia. *Inorganic Chemistry*, 59(2):1234-1241, 2019.

[26] Ruan, S., Lu, J., Pai, N., Ebendorff-Heidepriem, H., Cheng, Y. B., Ruan, Y., and McNeill, C. R. An optical fibre-based sensor for the detection of gaseous ammonia

with methylammonium lead halide perovskite. *Journal of Materials Chemistry C*, 6(26):6988-6995, 2018.

[27] You, X., Wu, J., and Chi, Y. Superhydrophobic silica aerogels encapsulated fluorescent perovskite quantum dots for reversible sensing of SO2 in a 3D-printed gas cell. *Analytical chemistry*, 91(8):5058-5066, 2019.

[28] Chen, C., Cai, Q., Luo, F., Dong, N., Guo, L., Qiu, B., and Lin, Z. Sensitive fluorescent sensor for hydrogen sulfide in rat brain microdialysis via CsPbBr3 quantum dots. *Analytical chemistry*, 91(24):15915-15921, 2019.

[29] Lin, F., Li, F., Lai, Z., Cai, Z., Wang, Y., Wolfbeis, O. S., and Chen, X. MnII-doped cesium lead chloride perovskite nanocrystals: demonstration of oxygen sensing capability based on luminescent dopants and host-dopant energy transfer. *ACS applied materials & interfaces*, 10(27):23335-23343, 2018.

[30] Chen, X., Hu, H., Xia, Z., Gao, W., Gou, W., Qu, Y., and Ma, Y. CsPbBr3 perovskite nanocrystals as highly selective and sensitive spectrochemical probes for gaseous HCl detection. *Journal of Materials Chemistry C*, 5(2):309-313, 2017.

[31] Xu, W., Li, F., Cai, Z., Wang, Y., Luo, F., and Chen, X. An ultrasensitive and reversible fluorescence sensor of humidity using perovskite CH 3 NH 3 PbBr 3. *Journal of Materials Chemistry C*, 4(41):9651-9655, 2016.

[32] Wu, P., He, Q., Zhu, D., Jiang, H., Jiao, Z., Zhang, Y., Xu, W., Fu, Y., Cao, H., and Cheng, J. Highly efficient fluorescent and colorimetric sensing of organic amine vapors based on organometal halide perovskite nanostructures. *Analytical Methods*, 9(25):3804-3809, 2017.

[33] Li, J., Du, P., Chen, J., Huo, S., Han, Z., Deng, Y., Chen, Y. and Lu, X. Dual-channel luminescent signal readout strategy for classifying aprotic/protic polar organic medium and naked-eye monitoring of water in organic solvents. *Analytical Chemistry*, 92(13):8974-8982, 2020.

[34] Liu, C. B., Sun, C. Y., Jin, L. P., and Lu, S. Z. Supramolecular architecture of new lanthanide coordination polymers of 2-aminoterephthalic acid and 1, 10-phenanthroline. *New Journal of Chemistry*, 28(8):1019-1026, 2004.

[35] Huang, H., Hao, M., Song, Y., Dang, S., Liu, X., and Dong, Q. Dynamic passivation in perovskite quantum dots for specific ammonia detection at room temperature. *Small*, 16(6):1904462, 2020.

[36] Petrochenkova, N. V., Mirochnik, A. G., Emelina, T. B., Sergeev, A. A., Leonov, A. A., and Voznesenskii, S. S. Luminescent amine sensor based on europium (III)

chelate. *Spectrochimica Acta Part A: Molecular and Biomolecular Spectroscopy*, 200:70-75, 2018.

[37] Li, G., She, C., Zhang, Y., Li, H., Liu, S., Yue, F., Jing, C., Cheng, Y., and Chu, J. A "Turn-on" fluorescence perovskite sensor based on $MAPbBr_3$/mesoporous TiO2 for NH3 and amine vapor detections. *Sensors and Actuators B: Chemical*, 327:128918, 2021.

[38] Huang, Y., Wang, S., Zhu, Y., Li, F., Jin, J., Dong, J., Lin, F., Wang, Y., and Chen, X. Dual-mode of fluorescence turn-on and wavelength-shift for methylamine gas sensing based on space-confined growth of methylammonium lead tribromide perovskite nanocrystals. *Analytical chemistry*, 92(8):5661-5665, 2020.

[39] Yan, J., Fu, Q., Zhang, S., Liu, Y., Shi, X., Hou, J., and Ai, S. A sensitive ratiometric fluorescent sensor based on carbon dots and CdTe quantum dots for visual detection of biogenic amines in food samples. *Spectrochimica Acta Part A: Molecular and Biomolecular Spectroscopy*, 282:121706, 2022.

[40] Jaiswal, S., Kundu, S., Bandyopadhyay, S., and Patra, A. A hybrid upconversion nanoprobe for ratiometric detection of aliphatic biogenic amines in aqueous medium. *Nanoscale Advances*, 3(11):3232-3239, 2021.

[41] Liu, Y., Xu, X., Lu, H., and Yan, B. Dual-emission ratiometric fluorescent probe-based lanthanide-functionalized hydrogen-bonded organic framework for the visual detection of methylamine. *Journal of Materials Chemistry C*, 10(4):1212-1219, 2022.